

pubs.acs.org/Macromolecules Article

# Characterizing the Areal Density and Desorption Kinetics of Physically Adsorbed Polymer in Polymer Nanocomposite Melts

Eric J. Bailey, Philip J. Griffin, Russell J. Composto, and Karen I. Winey\*



Cite This: Macromolecules 2020, 53, 2744-2753



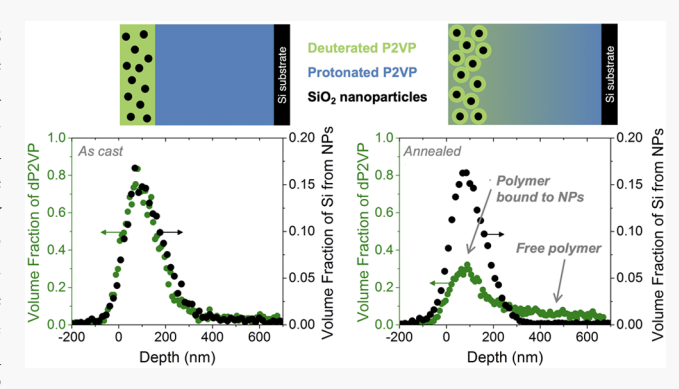
ACCESS

Metrics & More

Article Recommendations

Supporting Information

ABSTRACT: The interfacial regions between nanoparticles (NPs) and polymers in polymer nanocomposites (PNCs) underlie enhanced properties, and the temporal stability of these bound polymer layers is necessary for extended control on PNC performance. Using ion scattering techniques and poly(2-vinyl pyridine) (P2VP) mixed with 26 nm silica NPs, we investigate the lifetime of the bound polymer layer by separating and directly measuring the fraction of free polymer and polymer adsorbed to attractive NPs entirely in the melt state. By annealing thin PNC films deposited on bulk polymer matrices, free polymer from the PNC rapidly diffuses into the underlying matrix while the spontaneously formed bound polymer in the melt remains with the NPs. By correlating the fraction of bound chains with the NP



surface area, our analysis shows that bound polymer chains extend  $\sim R_{\rm g}$  from the NP surface into the melt. The calculated average NP surface area occupied by adsorbed chains in the melt is much smaller than predicted for an isolated chain or measured in an NP-polymer solution. The bound polymer fraction decreases as a function of annealing time and decreases more rapidly at higher temperatures and for lower molecular weights. This work demonstrates that ion scattering methods can quantitatively measure the chain-scale structure and dynamics of polymers bound to NPs in the melt state. This new information provides fundamental insights and enables the design of PNCs with greater thermal stability during fabrication and use.

## **■ INTRODUCTION**

Polymer nanocomposites (PNCs), or materials composed of nanoparticles (NPs) dispersed in a polymer matrix, are appealing candidates for a variety of applications and technologies, including functional materials, membranes and coatings, and various consumer products.1 In these materials, the polymer adsorbed to nanoparticles, often called the bound polymer, can enhance properties and improve NP dispersion, especially for PNCs with attractive NP-polymer interactions. 1-4 For example, this bound layer is responsible for mechanical strengthening<sup>5,6</sup> and improved ion and small molecule transport, 7,8 among other properties. In addition, the presence of bound layers can sterically prevent NP-NP aggregation, akin to a covalently grafted polymer brush but with less synthetic effort. 9-12 Importantly, the stability of the various PNC properties and NP morphology are predicated on the stability and lifetime of this bound layer, which remain poorly understood and challenging to measure. 1-3

The conformations of polymers adsorbed to interfaces are perturbed relative to bulk and contain trains (chains of adsorbed segments in direct contact with the surface), loops (sections of nonadsorbed segments between trains), and tails (nonadsorbed chain ends). As observed in various experiments, the bound polymer layer thickness ( $l_b$ ) around an NP in solution  $l_b$ 1,15,16 or in the melt  $l_b$ 1,17–19 is less than or

approximately the radius of gyration of the chain  $(R_{\rm g})$ . Molecular dynamics simulations reveal a similar length-scale and show that adsorbed chains have conformations that are flattened perpendicular to the NP surface and extend  $\sim R_{\rm g}$  from the NP surface. <sup>14,20</sup>

Polymer dynamics are also perturbed near NP-polymer interfaces.  $^{3,4,17,21-23}$  For example, in a mixture of poly(2-vinyl pyridine) (P2VP) and highly attractive silica (SiO<sub>2</sub>) nanoparticles studied by dielectric spectroscopy, P2VP segments beyond  $\sim$ 5 nm from the NP surface relax at timescales similar to bulk while P2VP segments within the bound layer relax nearly 100 times slower than in bulk.  $^{24,25}$  One may reasonably expect that these slow segmental relaxations lead to slow dynamics at longer lengths and timescales, an effect that has been observed near flat substrates.  $^{26-29}$  For example, polystyrene diffusion from a hydroxyl-covered silicon substrate was nearly one order of magnitude slower than in bulk, and

Received: October 18, 2019 Revised: January 27, 2020 Published: March 24, 2020





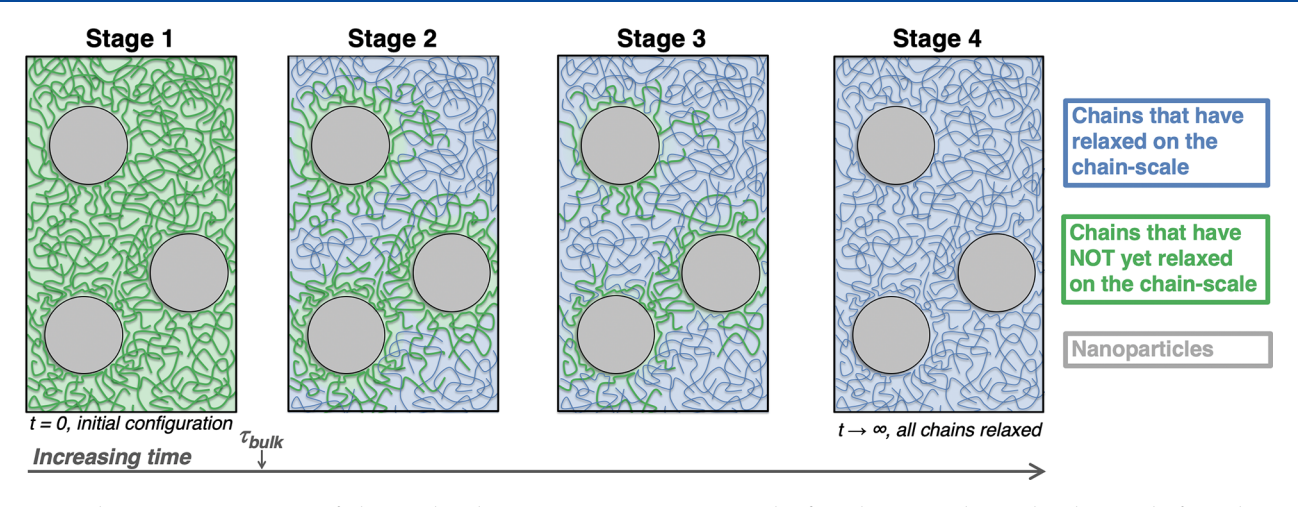


**Figure 1.** Schematic representation of chain-scale relaxations in attractive PNCs. The first chains to relax at the chain scale from the initial condition (Stage 1) are the bulk-like polymers far from an NP surface, while chains that are bound to the NP remain in their initial configuration (Stage 2). Next, chains that are loosely bound to the NP surface relax (Stage 3). Finally, at sufficiently long times, all chains have relaxed in Stage 4.

some chains remained immobile on the timescale of the experiment.<sup>26</sup> In the same system, solvent washing for up to 150 days revealed two populations of adsorbed chains: tightly bound chains composed predominately of trains and loosely bound chains composed predominately of loops and tails.<sup>28</sup>

Using this evidence of slow segmental dynamics near NPs in PNCs and heterogeneous populations of adsorbed chains at the substrate interface in thin films, it is reasonable to expect slow chain-scale dynamics at the NP interface in PNCs with attractive interactions. These anticipated populations are schematically represented in Figure 1. In the initial condition depicted in Stage 1, some chains reside in close proximity to the NP interfaces and others reside farther from NPs in bulklike regions. Free chains in the PNC, i.e., those far from the NP surface, are able to relax and diffuse at timescales similar to bulk chains. Thus, after annealing in the melt state on the order of the bulk chain mobility, this population of polymer will relax at the chain scale, diffuse, and be replaced by other free chains (Stage 2). At longer times, weakly bound chains, i.e., those with few or short trains, are expected to desorb from the NP surface and exchange with the free polymer. At this stage, only tightly adsorbed chains will remain from the initial PNC configuration (Stage 3). At sufficiently long times in Stage 4, even these tightly adsorbed chains will desorb so that all chains diffused relative to the initial configuration in Stage 1. Naturally, the timescales associated with these stages depend on various parameters such as NP size, polymer molecular weight, NP-polymer interactions, and temperature.

Distinguishing Stages 1–4 in PNCs remains an experimental challenge. By contrast, the directionality of thin films facilitates the separation of bound and free populations. However, some progress has been made in PNCs. For example, free chains can be removed by repeated solvent-washing, centrifuging to separate NPs with the adsorbed polymer from the free polymer, and then removing the free polymer.  $^{11,15,30,31}$  Recently, this technique was used to fabricate deuterated P2VP-coated SiO2 NPs that were dispersed in protonated P2VP and small-angle neutron scattering revealed a decreasing bound layer thickness with increased annealing time (i.e., from Stage 2 toward Stage 3).  $^{15}$  Interestingly,  $l_{\rm b}$  was found to decrease from  $\sim\!\!3$  to  $\sim\!\!0.6$  nm when annealing at  $T_{\rm g}$  + 75 °C, but  $l_{\rm b}$  remained constant after annealing at  $T_{\rm g}$  + 50 °C, indicating that the desorption process is highly temperature-

sensitive.<sup>15</sup> These scattering measurements sample the change in scattering length density, which depends on isotope concentration and local mass density<sup>19</sup> and subsequently assign a uniform bound layer thickness. Unfortunately, the extent to which the bound layer and interfacial polymer conformations are perturbed by solvent-washing, if at all, remains unclear. In another study with conventional sample preparation, the bound polymer layer thickness was inferred by measuring the SiO<sub>2</sub> NP diffusion in P2VP melts.<sup>37</sup> These measurements revealed an effective hydrodynamic radius larger than the core NP radius by  $\sim R_v$  implying that adsorbed chains remain adsorbed during NP diffusion.<sup>37</sup> Although the length scale of the bound polymer was determined and Stages 1 and 2 were distinguished, this NP diffusion study did not capture the internal structure or the stability of the bound polymer at long times. With limited data sets and few experimental methods, the understanding of chain-scale dynamics and properties of the bound layer in melt PNCs, and the dependence on various parameters, remains incomplete.

In this article, we develop ion scattering methods to quantify the fraction of bound and free polymers as a function of NP concentration, polymer molecular weight, annealing temperature, and annealing time. While most techniques define the bound layer through segment-sensitive properties 17-19,24,32,33 or rely on solvent-assisted separation of bound and free polymers, 9,11,15,16,28,31,34 the experiments presented herein probe the chain-scale structure and dynamics of bound polymers directly in the melt state. At short times (Stage 2), our analysis shows that bound chains extend  $\sim R_{\sigma}$  from the NP surface in the melt and reveal the average surface area per bound chain. The bound polymer fraction decreases at long annealing times and depends on annealing temperature and molecular weight. These results highlight the importance of chain-scale considerations on the structure and desorption dynamics in attractive PNC melts, motivate more investigations at the chain scale, and provide fundamental insights for stabilizing bound polymer layers.

## **■ EXPERIMENTAL SECTION**

**Materials.** The poly(2-vinylpyridine) (P2VP) polymers were purchased from Scientific Polymer Products and used as received. Partially deuterated poly(2-vinylpyridine), dP2VP, of 130 kg/mol was synthesized at the Center for Nanophase Materials Science at Oak

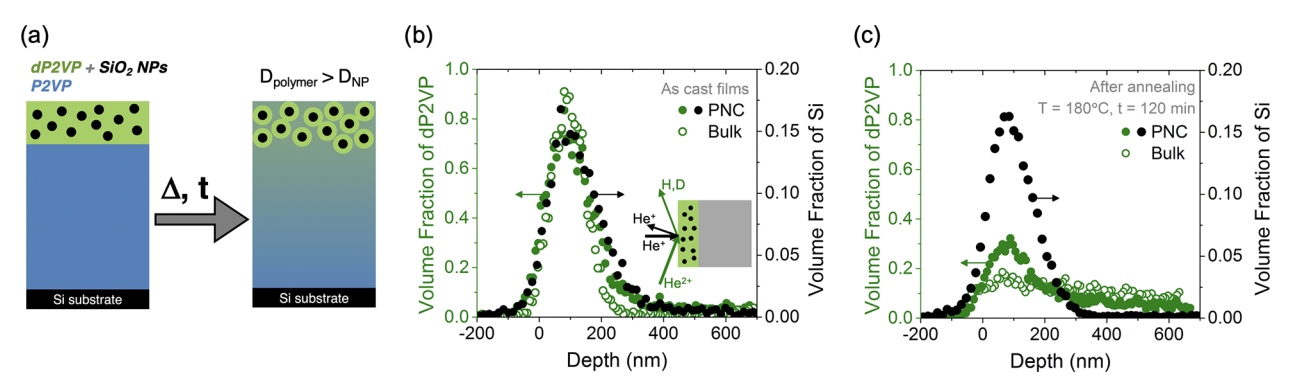


Figure 2. (a) Schematic representation of experimental samples before and after annealing. Blue and green represent P2VP and dP2VP, respectively, while black represents SiO<sub>2</sub> NPs. (b, c) ERD (green) and RBS (black) depth profiles for 110 kg/mol dP2VP samples with SiO<sub>2</sub> NPs (closed circles,  $\phi_{\rm NP}$  = 19 vol %) and without NPs (open circles) for samples before annealing (b) and after annealing for 120 min at  $T_{\rm g}$  + 80 °C (c). Inset of (b) depicts measurement geometry for ERD (green) and RBS (black). The underlying P2VP matrix in this representative dataset is 250 kg/mol. Schematics in (a) are not drawn to scale.

Ridge National Laboratory. Other dP2VP of 110 and 31 kg/mol were purchased from Polymer Source, Inc. and used as received. All polymer molecular weight averages that were characterized by GPC and polydispersities (compared to narrow polystyrene standards) are <1.4. We use  $T_{\rm g}=100~{\rm ^{\circ}C}$  for all P2VP and dP2VP samples. <sup>18</sup> Silica (SiO<sub>2</sub>) nanoparticles (NPs) were synthesized following the modified Stöber method <sup>35,36</sup> with a log-normal geometric mean diameter ( $d_{\rm NP}$ ) of 26.1 nm and standard deviation of 3.9 nm, as determined by analysis of transmission electron micrographs (TEM). <sup>37</sup>

**Bilayer Sample Fabrication.** Bilayer samples were composed of a thin (<150 nm) dP2VP-based PNC film deposited on a matrix of neat P2VP polymer, as depicted in Figure 2a. Neat P2VP matrices were made by doctor-blading a solution of P2VP in methanol (MeOH) ( $c_{\rm poly} \approx 50$  g/L) on an ozone-cleaned silicon wafer. Doctor-bladed films were dried for several hours at room temperature and then annealed at  $\sim T_{\rm g} + 80$  °C under vacuum for at least 48 h. The resulting films were  $\sim 20~\mu{\rm m}$  in thickness.

The PNC films were made from solution as follows. The dP2VP was mixed with MeOH and allowed to completely dissolve by stirring overnight. Then, requisite amounts of  $\mathrm{SiO}_2$  in ethanol (EtOH) were added to dP2VP/MeOH. The resulting polymer and NP concentrations were  $c_{\mathrm{poly}} < \sim 20$  g/L and  $c_{\mathrm{NP}} < 7$  g/L, respectively. This solution was stirred at room temperature for at least 48 h to ensure proper mixing and provide ample time for the spontaneous formation of the bound polymer layer in the solution.<sup>37</sup> To deposit the PNC films, a thin layer of 2000 kg/mol polystyrene (PS) was first spin-coated on an ozone-cleaned silicon wafer with a thickness  $\sim 30$  nm. This sacrificial PS layer mitigates potential  $\mathrm{SiO}_2$  aggregation at the polar substrate and promotes release of the adsorbing dP2VP PNC film from the wafer. The dP2VP/SiO<sub>2</sub>/MeOH PNC solution was then spin-coated onto the PS-treated silicon substrate to a thickness between 100 to 150 nm.

To form the bilayer samples (Figure 2a), the PNC film was lifted from the substrate in DI water (such that the PS layer is facing toward the water and the dP2VP layer is facing up) and transferred to the preannealed P2VP matrix. This diffusion couple is placed on a hotplate at  $T_{\rm g}$  + 50 °C for <20 s to weld the bilayer films and prevent delamination of the PNC film. Bulk diffusion couples (neat dP2VP on P2VP) that are used for comparison and to determine the diffusion coefficient of the free polymer are fabricated in the same manner as PNC tracer films, without the addition of NPs.

Bilayer films are annealed at the requisite temperatures under a nitrogen environment ( $\sim$ 0.4 atm) after at least four nitrogen purges. Temperature equilibration (within  $\pm 1$  °C) during purging was <1 min. For anneals less than 5 min, only one purge was used.

**Ion Beam Measurements.** The depth profile of dP2VP was measured using elastic recoil detection (ERD), which has been used to measure the tracer diffusion coefficient through the PNC film $^{38-41}$  and is described elsewhere. The Defense a depth resolution (full width at half-maximum) of  $\sim$ 110 nm and depth penetration (for

deuterium) of ~700 nm, which are large compared to both the NP and polymer size. In ERD,  $\mathrm{He^{2^+}}$  ions are accelerated at 3 MeV and incident onto the sample at  $70^\circ$  off-normal. Light elements, such as hydrogen and deuterium, are forward-recoiled to a detector at the complimentary angle. A thin (~10  $\mu$ m) Mylar film is used to block forward-recoiled  $\mathrm{He^{2^+}}$  ions. The measured energies are converted to depth profiles through the stopping power of  $\mathrm{He^{2^+}}$  into the sample, the stopping power of deuterium or hydrogen leaving the sample, and the stopping power through the Mylar film.

The depth profile of SiO<sub>2</sub> NPs was measured using Rutherford backscattering spectrometry (RBS), which has been used to measure the diffusion of tracer NPs into polymer matrices,  $^{37,38,40}$  as described elsewhere.  $^{38}$  RBS offers a depth resolution of  $\sim\!80$  nm and a penetration depth of  $\sim\!1~\mu\mathrm{m}$  (for Si). In RBS, He $^{+}$  ions are accelerated to 3 MeV and incident on the sample in normal geometry. Backscattered He $^{+}$  ions are collected at a detector 10° off-normal. The energies of collected He ions are converted to depth profiles by the stopping power of He $^{+}$  into and out of the sample.

## RESULTS

Evidence of Bound Polymer. Figure 2 shows a schematic representation of the experimental samples and process (Figure 2a) and representative experimental data (Figure 2b,c). As shown in Figure 2b, the as-cast PNC bilayer samples contain a mixture of dP2VP (solid green) and SiO<sub>2</sub> NPs (black) in the top ~150 nm film. We selected material systems and annealing conditions such that  $D_{\mathrm{NP}}$  <  $D_{\mathrm{poly}}$ . Therefore, after short annealing times, the NPs remain in the top ~150 nm (Figure 2c, black), while the free polymer diffuses into the underlying matrix (Figure 2c, green). Compared to the diffusion of neat dP2VP (Figure 2c, open circles), the PNC bilayer sample annealed at the same conditions contains excess dP2VP in the top film (where the NPs are located) and a corresponding depletion of dP2VP beyond ~200 nm. These data clearly demonstrate the ability of these experiments to separate the dP2VP that quickly diffuses away from the PNC layer and the dP2VP that is slower to diffuse and thereby establish the timescale for Stage 2. Analysis of these profiles reveals the amount of bound polymer, and by extending to longer anneals, the progression from Stage 2 to Stage 3.

Extracting the Fraction of Bound Chains. Akin to Figure 1, the analysis of the dP2VP depth profiles considers two populations: bound polymer residing in the top PNC film  $(\phi_{\rm bound})$  and free polymer diffusion into the matrix  $(\phi_{\rm free})$ . Thus, the depth profiles are fit to a linear combination of

 $\phi_{
m bound}$  and  $\phi_{
m free}$  that is convoluted with a Gaussian representing experimental resolution.

$$\phi(z) = \text{Res} \times \{\phi_{\text{bound}}(z) + \phi_{\text{free}}(z)\}$$
 (1)

where

$$\phi_{\text{bound}}(z) = X_{\text{bound}} \times \phi_{\text{poly}} \text{ when } 0 < z < h$$
 (2)

$$\phi_{\text{free}}(z) = (1 - X_{\text{bound}}) \times \left(\frac{1}{2} \left[ \text{erf} \left( \frac{h - z}{\sqrt{4Dt}} \right) + \text{erf} \left( \frac{h + z}{\sqrt{4Dt}} \right) \right] \right)$$
(3)

where z is the depth, Res is the resolution function,  $\phi_{\text{poly}}$  is  $1-\phi_{\text{NP}}$ , h is the thickness of the PNC film, D is the free chain diffusion coefficient, t is the annealing time, and  $X_{\text{bound}}$  represents the number fraction of bound dP2VP chains. A representative fit is provided in Figure 3a.

A step function is used to describe the deuterated polymer in the PNC layer (eq 2), which after annealing is the signature of the bound polymer. The  $\phi_{\text{poly}}$  and h values in eq 2 are known from RBS and ERD measurements of the unannealed bilayer sample (Figure S2). The concentration profile of the free polymer is described by eq 3 and is the solution to Fick's second law for a finite source diffusing into a semi-infinite medium, as previously reported. 37,39,40 The diffusion coefficient of neat dP2VP into the P2VP matrix (D<sub>bulk</sub>, Figure S4) is used to approximate the diffusion of free dP2VP chains through the NPs in the PNC layer and in the underlying matrix. Note that the D used to fit the annealed PNC bilayer samples may be reduced from the bulk diffusion coefficient by at most ~25% to improve the fit to ERD data. 39,42 In addition, the tracer PNC film thickness, h, may vary upon annealing due to asymmetric diffusion between dP2VP and P2VP, i.e., the Kirkendall effect. 43 Thus, the thickness in eq 2 is allowed to vary between the resolution of ERD (~110 nm) and the ERDmeasured thickness of unannealed samples, typically 125-150 nm. Importantly, these two parameters (D and h) can be separately evaluated because they have distinct contributions to the overall depth profile of dP2VP. Thus, after selecting the appropriate D (0.75· $D_{\text{bulk}} \leq D \leq D_{\text{bulk}}$ ) based on the slope at z> 200 nm, h is selected by the region 100 < z < 200 nm. As a result,  $X_{\text{bound}}$  is the only remaining fit parameter used to describe the relative concentrations at z < 200 nm (bound polymer) and z > 200 nm (free polymer).

It is important to note that  $X_{\text{bound}}$  is explicitly defined as the excess dP2VP fraction residing with the NPs in the thin PNC layer after a given annealing time and not necessarily the fraction of chains in direct contact with the NP surface. However, at short annealing conditions, the rate limiting step for polymer diffusion into the underlying matrix is most likely desorption from the attractive NP rather than slow diffusion through the PNC film (i.e., confinement effects imposed by NPs). Previous studies have established that the reduction in polymer diffusion coefficient (relative to bulk) through comparable PNCs is dependent on the interparticle distance (ID)<sup>44</sup> relative to the chain size  $(2R_g)$ . <sup>39,42</sup> For the most confining PNC conditions studied herein, the tracer diffusion is expected to be only ~2 times slower than the bulk polymer.<sup>39,42</sup> Furthermore, this anticipated slow diffusion of the free polymer in the PNC lasts only in the PNC film, which is ~150 nm in total thickness. In reality, the population

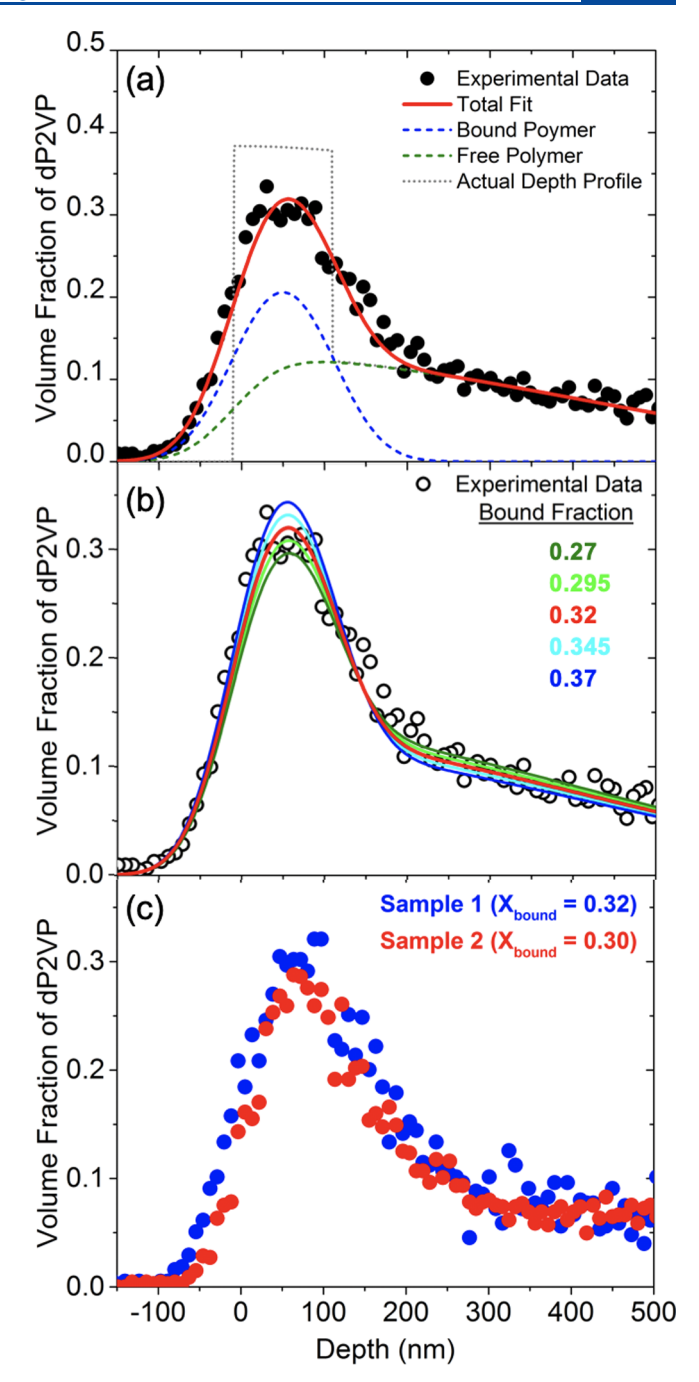


**Figure 3.** (a) Representative volume fraction of dP2VP as a function of depth (circles), total fit (red solid line), contributions from bound polymer (blue dashed line) and free polymer (green dashed line), and the actual depth profile without experimental resolution (gray dotted line). (b) Comparison of fit quality for various values of  $X_{\rm bound}$ , where the limits are considered poor fits, to demonstrate fitting errors. (c) Comparison of duplicate samples and measurements showing reproducibility. Data displayed is for 110 kg/mol dP2VP deposited on 250 kg/mol P2VP,  $\phi_{\rm NP}$  = 19 vol %,  $T = T_{\rm g} + 80$  °C, and t = 45 min (a, b) or 180 min (c).

described by  $\phi_{\rm bound}$  diffuses orders of magnitude slower than the bulk. Thus, when chains desorb, they are able to freely diffuse into the underlying matrix, thereby leading to the experimental realization of Figure 1.

Finally, the extracted values of  $X_{\text{bound}}$  may have uncertainties associated with fitting the model or sample-to-sample

variability. Figure 3b shows how the fit varies from experimental data for different values of  $X_{\rm bound}$  with other variables fixed. We consider  $X_{\rm bound}=0.32$  as the best fit, but shows a variance of  $\pm 0.05$ , where the extremes clearly deviate from the concentration profiles, particularly at z=75 and 250 nm. Figure 3c shows replicated samples under the same conditions to demonstrate small variances between identical samples. Thus, we estimate an error bar of  $\pm 0.03$  on  $X_{\rm bound}$ .

**Effect of NP Concentration.** To explore the role of NP concentration  $(\phi_{\rm NP})$ , we measure the depth profile of dP2VP-130 (130 kg/mol dP2VP) with SiO<sub>2</sub> NP concentrations of 4, 11, and 16 vol %. All samples were annealed for 45 min at 180 °C ( $\sim T_{\rm g} + 80$  °C), and the underlying matrix was 110 kg/mol P2VP. At these annealing conditions, the characteristic diffusion length of neat dP2VP-130 is more than 500 nm. Thus, the free polymer diffuses into the underlying film during annealing (Figure 4a), while the slower NPs and the NP-bound polymer remain near the surface (Figure 4b).

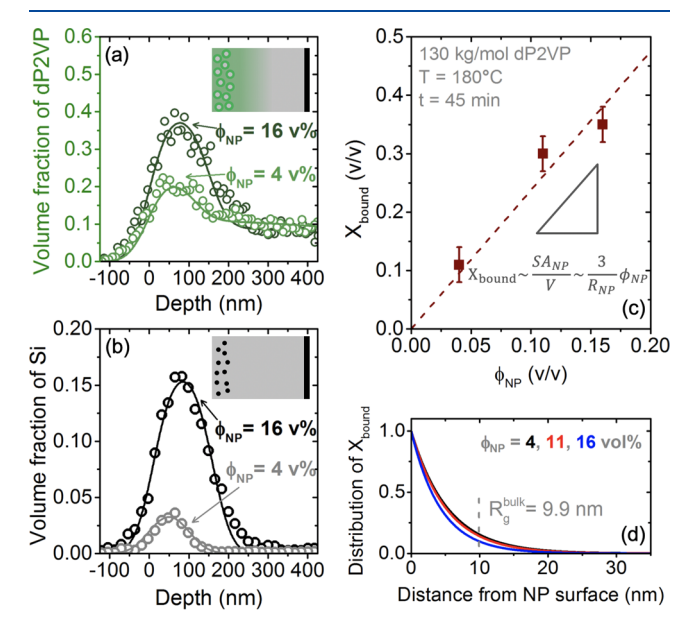


Figure 4. (a) ERD measurements of dP2VP-130 concentrations and (b) RBS measurements of NP concentrations as a function of depth after annealing PNC samples of  $\phi_{\rm NP}$  = 4 vol % (light) and 16 vol % (dark) for 45 min at T=180 °C. (c)  $X_{\rm bound}$  as a function of  $\phi_{\rm NP}$  showing linear dependence. (d) Extracted concentration of bound polymer as a function of distance from the NP surface (assuming exponentially decaying distribution) showing a bound layer thickness on the order of  $R_{\rm g}$ . The underlying P2VP matrix is 110 kg/mol.

As shown in Figure 4c, the extracted  $X_{\rm bound}$  of dP2VP increases linearly with the NP concentration from the origin. In PNCs with individually dispersed NPs, the bound fraction is expected to scale linearly with the NP surface area and thereby with  $\phi_{\rm NP}$ . Thus, the linear relationship in Figure 4c is consistent with our assertion that  $X_{\rm bound}$  reflects the polymers adsorbed to the NP surface, as depicted in Stage 2. Note that  $X_{\rm bound}$  is ~34% at  $\phi_{\rm NP}$  = 16 vol %, indicating that the majority of polymer chains are free to diffuse and relax at timescales similar to the neat polymer.

To gain more insight into the quantitative meaning of  $X_{\rm bound}$ , the concentration profile of the bound polymer around a single NP can be calculated by assuming an exponential decay as a function of distance from the NP surface. Using a construct with a single NP in a volume defined by  $\phi_{\rm NP}$  and

 $R_{\rm NP}$ , the bound polymer ( $X_{\rm bound}$ ) was represented by spherically integrating the exponential profile around the NP surface

$$X_{\text{bound}} = \frac{4\pi \int_{R_{\text{NP}}}^{\infty} r^2 e^{-(r - R_{\text{NP}})/l_b} dr}{\frac{4}{3}\pi R_{\text{NP}}^3 \left(\frac{1 - \phi_{\text{NP}}}{\phi_{\text{NP}}}\right)}$$
(4)

where  $l_{\rm b}$  is the characteristic length of the exponential decay of the bound polymer concentration. Figure 4d shows the extracted concentration profiles of the bound layer. The bound layer extends  $\sim R_{\rm g}$  from the NP surface with  $l_{\rm b} \approx 4.9 \pm$ 0.7 nm. This value of  $l_b$  is independent of  $\phi_{\rm NP}$ , as expected, and is smaller than the chain size  $(R_{\rm g} \approx 9.9~{\rm nm}^{15,37})$ , in agreement with other measurements of the bound layer thickness. 3,11,15,37 The result that  $l_b \leq R_g$  further supports our assertion that (i) annealing at 180 °C for 45 min is sufficient for the free polymer to spatially separate from the NP-bound polymer, i.e., Stage 2, and (ii) that our definition and extraction of  $X_{\text{bound}}$ accurately reflect the bound fraction. In addition, the result that  $l_{\rm b}$  is independent of  $\phi_{\rm NP}$  suggests that polymer bridging has little effect on our results, despite the fact that polymer bridging has been observed through mechanical measurements at small NP concentrations  $(\phi_{\rm NP}$  < 5 vol %)<sup>45</sup> and that ID at 16 vol % ( $\sim$ 16.2 nm)<sup>44</sup> is slightly smaller than  $2R_g$  (19.8 nm).

**Desorption of Bound Polymer.** The diffusion of free dP2VP into the underlying P2VP matrix is relatively rapid (<1 h), as demonstrated in the experimental realization of Stage 2 in Figure 4. However, polymers that are initially adsorbed to NPs may desorb and become free to diffuse at longer times (Stages 3 and 4). Inportantly, the NP diffusion must be restricted to access sufficiently long annealing times. To impede NP diffusion (Figure S5) without perturbing free polymer diffusion,  $^{39,46}$  the underlying P2VP  $M_{\rm w}$  was increased from 110 to 250 kg/mol.  $^{37,47,48}$ 

First, we measure the bound fraction remaining in the PNC after long annealing times in an effort to observe Stage 4. Figure 5b presents measurements of PNCs composed of dP2VP-31 and dP2VP-110 with  $\phi_{\rm NP}=19$  vol % deposited on 250 kg/mol P2VP after  $\sim$ 12 h of annealing at 160, 180, and

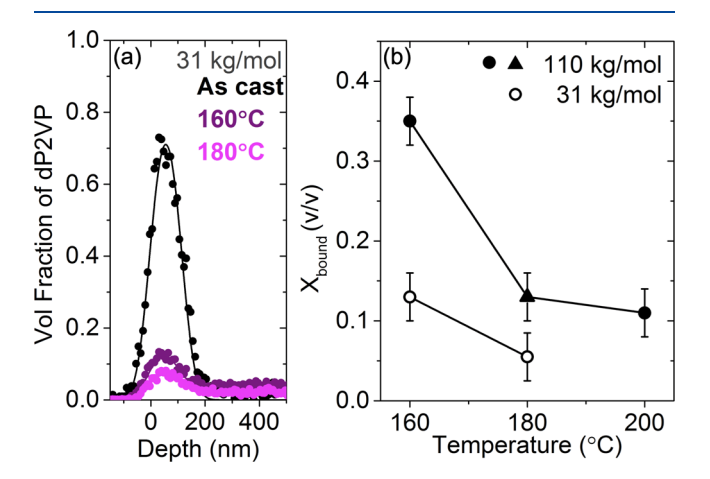


**Figure 5.** (a) Depth profiles for dP2VP-31 that are unannealed (black) and annealed at 160 °C (purple) and 180 °C (magenta) for 12 h. (b) Measured  $X_{\rm bound}$  for dP2VP-31 (open symbols) and dP2VP-110 (closed symbols) as a function of annealing temperature for annealing times of 12 h (circles) or 13 h (triangle). The P2VP matrix is 250 kg/mol and the PNC layer has  $\phi_{\rm NP}=$  19 vol %.

200 °C. Importantly, all dP2VP depth profiles show the presence of bound polymer, meaning that Stage 4 is not observed under these experimental conditions. For all temperatures studied, dP2VP-31 exhibits a lower bound fraction than dP2VP-110, which is consistent with smaller  $l_{\rm b}$  expected for lower  $M_{\rm w}$ . For a fixed annealing time (~12 h), more polymer desorption has occurred at higher temperatures. Although we observe a sharp decrease in  $X_{\rm bound}$  between 160 and 180 °C, only a modest decrease in  $X_{\rm bound}$  is observed upon further increasing the temperature to 200 °C.

To probe the kinetics of desorption, i.e., the transition from Stage 2 to Stage 3,  $X_{\text{bound}}$  was measured as a function of annealing time. As shown in the depth profiles for dP2VP-31 (Figure 6a) and dP2VP-110 (Figure 6b), the dP2VP

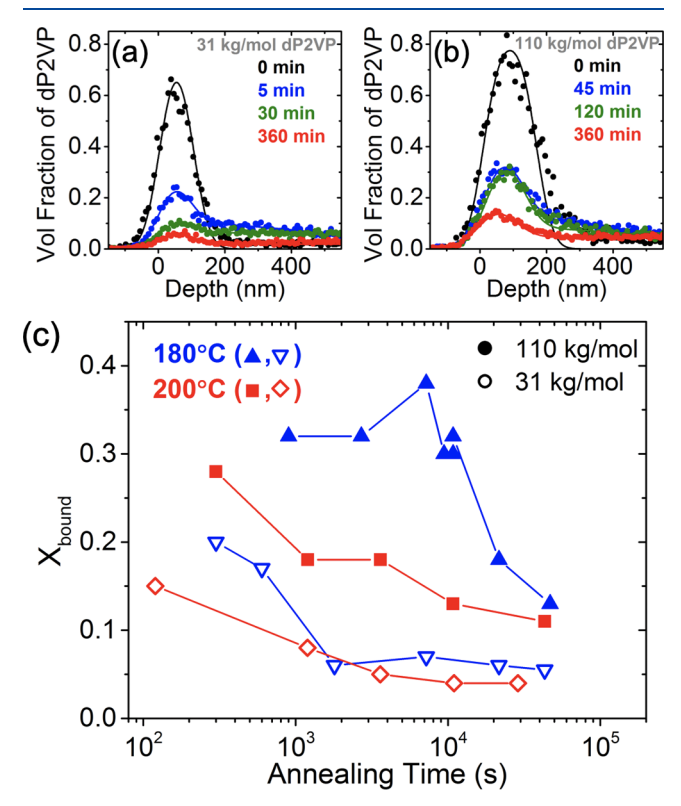


**Figure 6.** ERD depth profiles for (a) dP2VP-31 and (b) dP2VP-110 for various annealing times for T=180 °C. (c) Extracted  $X_{\rm bound}$  as a function of time. The P2VP matrix is 250 kg/mol and the PNC layer has  $\phi_{\rm NP}=19$  vol %. Error bars of 0.03 in (c) are omitted for clarity.

concentration in the top PNC layer generally decreases as the annealing time increases. For dP2VP-31 and dP2VP-110 annealed at 180 and 200 °C, the extracted  $X_{\rm bound}$  are plotted in Figure 6c as a function of annealing time. Figure 6c shows a systematic decrease in  $X_{\rm bound}$  with increasing annealing time and demonstrates ongoing dP2VP desorption from SiO<sub>2</sub> NPs. Furthermore, for these times, smaller values of  $X_{\rm bound}$  are observed for the lower  $M_{\rm w}$  dP2VP-31 (open circles) and at higher temperatures (red symbols), consistent with Figure 5b. For dP2VP-31, after an initial decrease in  $X_{\rm bound}$  upon annealing, a plateau of  $X_{\rm bound}$   $\approx$  5% is observed at both 180 and 200 °C. For longer dP2VP-110 at 180 °C, the initial  $X_{\rm bound}$  persists and a decrease in  $X_{\rm bound}$  occurs at longer annealing times. Thus, we observe slower desorption kinetics for larger polymers and at lower temperatures.

In summary, at short annealing times as demonstrated in Figure 4, we experimentally separate and identify bound polymer from the free polymer (Stage 2). Then, upon further annealing, as demonstrated in Figure 6c, we observe polymer desorption from Stage 2 to Stage 3. Although the rate at which chains desorb depends on  $M_{\rm w}$  and temperature, in all cases, polymers that are initially bound become free after additional annealing. At long times (as demonstrated in Figures 5 and 6c), some polymer remains adsorbed to the NPs in each data set, meaning that complete desorption (Stage 4) was not observed at these experimental conditions.

## DISCUSSION

## Ion Beam Methods to Probe Bound Polymer in PNCs.

Before further discussing the results presented above, this section will highlight the advantages and challenges of combining ERD and RBS to measure the static and dynamic properties of bound polymer in PNCs. These ion scattering methods are unique in that they measure the chain-scale structure and dynamics of bound polymer by isolating and quantifying the bound polymer directly in the melt. Previous studies have probed chain-scale mobility of polymers (polymer diffusion) in PNCs<sup>39,40,42</sup> and other studies have probed segmental dynamics at the NP interface, <sup>24,25</sup> but a few studies have probed chain-scale phenomena at the interface. <sup>11,15,37</sup> In addition, many studies that probe the bound polymer layer use solvent to isolate the bound polymer layer, which may change the polymer conformations of the bound layer relative to the melt. <sup>11,15,16</sup> Below, we summarize the unique attributes and limitations of these measurements.

Conventional PNC Fabrication Methods. PNC samples for these ion beam measurements are fabricated by conventional solvent-based fabrication procedures so that the observations are widely applicable. To be specific, we mix a single polymer component with solvent and NPs and spin-coat the film. Thus, the bound layer is formed naturally and spontaneously in solution and densified as solvent is removed. All postprocessing is conducted in the glassy state and separation of bound and free polymers is done purely in the melt state.

Separate Free and Bound Polymers. Using the sample geometry in Figure 2a, isolation of free and bound polymers is achieved by the comparatively faster diffusion of free polymers from the PNC layer into the homopolymer layer. This spatial separation of free and bound polymers, as discussed in Figure 3, enables straightforward data interpretation using the simple model presented in eq 1. The ability to selectively and independently measure the depth profile of the NPs (RBS) and deuterated polymer (ERD) in various samples and for different annealing conditions (t,T) permits informed fitting of experimental data and, ultimately, accurate delineation of bound and free polymers.

Measurement of Bound Fraction. This ERD/RBS measurement directly measures the amount of bound polymer in the PNC, as opposed to a length scale of the bound layer or the local dynamics within it. As a result, new information is available. Although straightforward approximations can lead to the bound layer thickness (Figure 4d and Figure S3) and measurements as a function of time can lead to chain-scale dynamics (Figure 6c), additional information such as the average NP surface area occupied by adsorbed chains can be reported (as discussed below). Note that this method, unlike scattering methods or measurements of hydrodynamic sizes, is not sensitive to the size, shape, or size dispersity of the NPs.

However, the experimental signal depends intimately on the interfacial area, which presents an inherent paradox: high NP concentrations are desired to maximize the signal in the measurement and low NP concentrations are desired so adjacent NPs are noninteracting and polymer bridges between different NPs are minimized. Thus, a good practice is to measure the bound layer at multiple NP loadings (Figure 4).

Broad Potential for Studying Experimental Parameters. This experimental method offers a wide array of accessible experimental parameters, many of which were studied herein, such as temperature, time,  $M_{
m w}$ , and  $\phi_{
m NP}$ . Ex situ annealing provides a wide range of time and temperature without complicating the ERD/RBS measurements. The two main requirements for the PNC system are the necessity of deuterated polymer and slower NP diffusion than polymer chain diffusion. For the former, it is important to note that partially deuterated polymer can be used and that these measurements require very little deuterated polymer ( $\sim$ 10  $\mu$ g per sample). For the latter,  $D_{NP} < D_{poly}$  is naturally true for many annealing conditions and several PNC systems. When necessary, the NP diffusion can be slowed down by increasing the viscosity or even lightly cross-linking the underlying matrix (e.g., Figure S5). For matrix materials that significantly differ from the tracer polymer, it will be important to characterize how the differences impact the measurement. Although not a requirement, these ERD/RBS measurements are more convenient for glassy polymers (i.e.,  $T_{\rm g}$  < 25 °C). Beyond these straightforward requirements to the materials, the ERD/ RBS method is applicable to a broad range of PNC systems and experimental parameters.

Measuring Concentration Profiles. The ability to quantify the polymer and NP concentrations as a function of depth into the sample is critical to the success of these measurements. Here, we use ERD and RBS measurements that require specialized equipment not commonly available. Other techniques that are more widely available, such as secondary ion mass spectrometry, are likely capable of similar measurements of the bound layer in PNCs. Depth-profiling techniques are insensitive to areal information so complimentary measurements might be needed to probe areal properties (e.g., NP dispersion).

Characterization of Areal Density. With direct measurement of the number fraction of bound chains  $(X_{\rm bound})$  and precise knowledge of the NP surface area (through  $R_{\rm NP}$  and  $\phi_{\rm NP}$ ), we can report the average surface area occupied by an adsorbed chain, a parameter that is often difficult to quantify in the melt. At 180 °C, about 32% of the dP2VP-110 remains as bound polymer after 45 min (Figure 6c). These annealing conditions are identical to those in Figure 4c and were long enough to separate free and bound polymers but short enough to minimize desorption of initially bound dP2VP (Stage 2), as supported by the extracted bound polymer layer thickness (Figure S3). The measured  $X_{\rm bound}$  values can be related to the total NP surface area to reveal the average NP surface area occupied by each dP2VP chain ( $(SA_{\rm chain})$ )

$$\langle SA_{chain} \rangle = \left(\frac{3}{R_{NP}}\right) \left(\frac{\phi_{NP}}{1 - \phi_{NP}}\right) \left(\frac{M_{w}}{X_{bound}\rho_{poly}N_{A}}\right)$$
(5)

where  $\rho_{\rm poly}$  is the neat polymer mass density and  $N_{\rm A}$  is Avogadro's number. Equation 5 assumes all bound chains are dP2VP. Note that at longer annealing times where dP2VP/

P2VP exchange is likely, calculating  $\langle SA_{chain} \rangle$  is unreliable and therefore not reported.

For dP2VP-110,  $\langle SA_{chain} \rangle$  is ~14 nm<sup>2</sup>/chain in the melt state, which corresponds to an effective areal density of 0.072 chains per nm<sup>2</sup>. For comparison, the projected areal coverage of an unperturbed polymer  $(\pi R_g^2)$  isolated on the NP surface is much larger  $\langle SA_{chain} \rangle \approx 260 \text{ nm}^2/\text{chain}$ . This result suggests that the adsorbed dP2VP has relatively few (or short) trains and several (or large) loops and tails. Moreover, this areal density highlights that bound chains are highly interpenetrating within the bound layer. In contrast, a similar P2VP/SiO<sub>2</sub> system was repeatedly solvent-washed to remove the free polymer and is reported to have a polymer concentration of ~12 wt %, corresponding to  $\langle SA_{chain} \rangle \approx 60 \text{ nm}^2/\text{chain.}^{15}$  The smaller (SA<sub>chain</sub>) measured by ion scattering in the melt appears to be the result of solvent washing producing less bound polymer than in the melt. This observation can be reconciled in terms of the polymer density in the bound layer. For an isolated chain, since the polymer density is low, the chains near the interface occupy more of the surface area. As the polymer density increases in a polymer solution and more so in the melt, the densification leads to more polymers near the interface and therefore more that are bound. This quantitative comparison further highlights the differences between the bound layer in solution and in the melt.<sup>11</sup>

For dP2VP-31, (SA<sub>chain</sub>) is 5.8 nm<sup>2</sup>/chain (areal density of 0.17 chains per nm<sup>2</sup>) at the shortest annealing time accessible at 180  $^{\circ}\text{C}$  (5 min). The measured  $\langle SA_{chain} \rangle$  relative to the projected chain size,  $\langle SA_{chain} \rangle / \pi R_g^2$ , are 8.0 and 5.3% for dP2VP-31 and dP2VP-110, respectively. This difference suggests that a larger percentage of segments in dP2VP-31 chains are adsorbed on the surface of the NP. This observation is consistent with the model previously proposed from broadband dielectric spectroscopy (BDS), pycnometry, SAXS, and IR and X-ray spectroscopy studies, which indicate that shorter chains pack more efficiently at an interface. 17,25 It is also somewhat surprising that the chains in both PNCs occupy, on average, relatively small amounts of the NP surface yet still exhibit long-lived adsorption. Although we begin to interpret these dynamic results further in the next section, it is important to note that our analysis of (SA<sub>chain</sub>) reveals an average areal density and whether the distribution is narrow, broad, or multimodal remains unclear. As others have discussed,  $^{3,11,15,28}$  we expect the  $\langle SA_{chain} \rangle$  of individual chain can deviate strongly from the average and can be phenomenologically described as ranging from weakly to strongly adsorbed.

Collapse of Desorption Data. Data in Figure 6c characterizes the desorption of bound polymer as a function of time for different annealing temperatures and  $M_{\rm w}$ . To gain insights into the mechanism and microscopic parameters that influence the lifetime of the bound layer, we scale the annealing time to different polymer dynamic processes. Since the P2VP/SiO<sub>2</sub> interaction and adsorption are fundamentally at the segment scale, Figure 7a shows  $X_{\text{bound}}$  as a function of annealing time normalized by the segmental relaxation time,  $\tau_{\alpha}$ , of the neat polymer (obtained from ref 18). Although the data from 180 and 200 °C seem to overlay on each other,  $\tau_{\alpha}$  fails to capture the effect of  $M_{\rm w}$ , suggesting that bound polymer desorption also requires consideration of polymer chain length or cooperative motion. Since this measurement fundamentally monitors the diffusion of the chain from the NP surface, Figure 7b shows  $X_{\text{bound}}$  as a function of annealing time normalized by

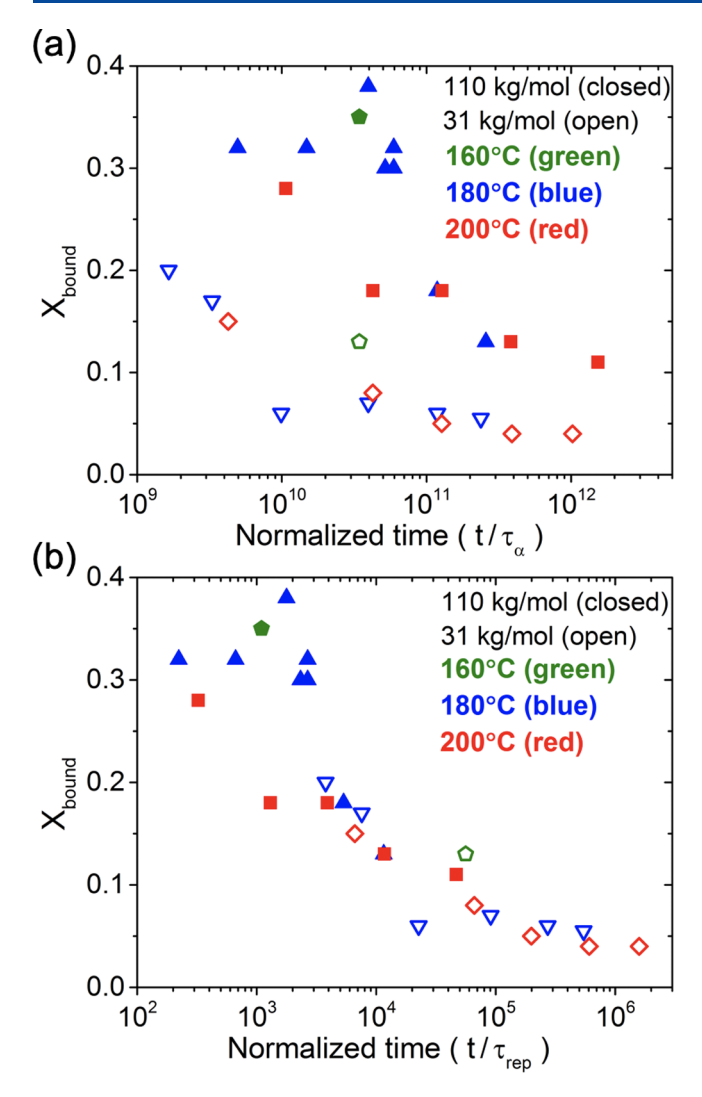


**Figure 7.** Rescaled desorption data from Figure 6c. The experimental  $X_{\text{bound}}$  is plotted as a function of (a) annealing time normalized to segmental relaxation time  $(\tau_{a})$  and (b) annealing time normalized to chain reptation time  $(\tau_{\text{rep}})$ .

the chain-scale mobility, given by the reptation time in bulk polymer ( $\tau_{\rm rep} = R_{\rm g}^2/D_{\rm chain}$ , Supporting Information). The  $X_{\rm bound}$  data for two molecular weights, three annealing temperatures, and a range of annealing times collapse reasonably well. Note that error bars of  $\pm 0.03$  on  $X_{bound}$  are omitted for clarity. The current data set spans a range of 10<sup>2</sup>- $10^6 \tau_{rep}$  and the bound fraction decreases by nearly 6 times, from  $\sim 30$  to  $\sim 5\%$ , over that timescale. On average, these chains desorb  ${\sim}10^4$  times slower than bulk  $\tau_{\rm rep}$  but even after annealing for times longer than  ${\sim}10^6~\tau_{\rm rep}$ , some polymer remains adsorbed. Chain desorption occurring after more than  $10^{10}$   $au_{lpha}$  or  $10^3$   $au_{
m rep}$ , if they desorb at all, is particularly noteworthy considering the relatively small average (SA<sub>chain</sub>) we calculated using eq 5. We speculate that the chains with relatively few adsorbed segments (and therefore lower local SA<sub>chain</sub>) are the ones we observe desorbing while those with more absorbed segments (and therefore higher local SA<sub>chain</sub>) are the bound chains that persist beyond  $\sim 10^6 \tau_{\rm rep}$ . It remains unclear how the polymer conformations and distribution of them within the bound layer change during annealing, desorption, resorption, and exchange.

While it remains to be tested if this collapse will apply to a broader range of PNCs and conditions, the effective collapse of the current data implies significant cooperativity and chain length dependence of desorption of P2VP from SiO<sub>2</sub>. The observed correlation between polymer desorption and  $t/\tau_{\rm ren}$  in Figure 7b highlights two important dependences: temperature and chain length. The temperature dependence is largely captured by the temperature dependence of polymer dynamics (i.e., friction coefficient) as opposed to an activation energy. In fact, normalization of the annealing time to either  $au_{lpha}$  or  $au_{
m rep}$ reasonably collapses data from the same  $M_w$ , which is consistent with the fragility of chain-scale and segmental mobilities often being comparable.<sup>49</sup> The desorption kinetics may become decoupled from polymer dynamics as the temperature approaches  $T_g$ , but desorption will slow precipitously and may be experimentally inaccessible. The dependence of desorption on chain length, where  $t/\tau_{\rm rep} \approx N^3$ for entangled chains, could be influenced by the fact that larger chains have (i) slower intermediate and chain dynamics in bulk, (ii) more adsorbed segments per chain, and (iii) likely more or longer trains per chain. It is important to note that all polymers in our measurements are entangled  $(M > M_e)$ , and although it remains unclear how the entanglement network and constraint release is perturbed in the bound layer, 37,40,50 this may contribute to the observed chain-length dependence in Figure 7.

Our results clearly demonstrate that polymer desorption from attractive NPs in the melt is more than a segmental phenomenon, is cooperative in nature, and is complex. Despite our observation in Figure 7, it remains unclear if desorption is dictated by a segmental relaxation rate and chain-length dependent adsorption energy or, conversely, a chain-scale relaxation rate and a chain-length independent adsorption energy. One may reasonably expect the timescale of desorption to be related to the product of a segmental relaxation time and exponential of the adsorption energy. In this light, one can imagine incorporating another term into the normalization of Figure 7a that accounts for an adsorption energy that changes with molecular weight. This difference in adsorption energy may result from a different average length of trains, distribution of loops and trains, or reflect some longer-lasting cooperativity. The current data set is insufficient for this level of analysis or the definition of this adsorption energy. Alternatively, the collapse in Figure 7b may suggest that the chain-scale relaxation plays a dominant role and the effective energy term is on the order of  $\sim 10^4$  and constant with the molecular weight. A physical interpretation of this may be that the rate limiting step for desorption is chain diffusion away from the NP surface. In other words, interfacial segments can desorb and readsorb (which occurs on the order of  $10^{-5}$  s according to BDS)<sup>17,24</sup> until the chain diffuses away from the NP surface (which occurs on the order of 10<sup>3</sup> s according to Figure 6c). Although our results in Figure 7 begin to interrogate the complex and multiscale questions associated with polymer desorption from an NP surface, many answers remain elusive. Future experimental and theoretical efforts are required to provide more insight into the underlying physics, development of a mechanistic description, and documentation of the microscopic properties and parameters that dictate bound layer desorption in polymer melts.

## CONCLUSIONS

The combination of ERD and RBS experiments separates, identifies, and quantifies spontaneously formed bound polymer layers in polymer nanocomposite melts and reveals new static and dynamic properties of bound polymers. Unlike most measurements of bound polymers in PNCs that rely on solvent-assisted removal of free chains<sup>9,11,15,16,28,31,34</sup> or define bound and free polymers through segment-sensitive techniques, 17–19,24,32,33 these ion scattering methods define the bound layer in the melt through deviations in the chain-scale dynamics. Three populations of chains are observed in our measurements: free chains diffusing at bulk-like timescales, weakly adsorbed chains that desorb at timescales  $\sim 10^4$  times slower than bulk polymer diffusion, and strongly adsorbed chains that remain bound for these experimentally accessible timescales. These ion scattering measurements reveal a bound layer thickness of  $\sim 0.5R_{\rm g}$ , that bound polymer extends  $\sim R_{\rm g}$ from the NP surface, and the average surface area occupied by bound chains in the melt, which is much smaller than predicted by an isolated chain model or measured in solution. Polymer desorption increases with annealing time and the polymer desorption kinetics depends on temperature and chain length. This study provides a framework to understand bound polymer structure and desorption in the melt and to guide the design and evaluation of more stable interfacial layers. Our results and observations motivate theoretical and further experimental inquiries into the kinetics and mechanisms of polymer desorption from NPs and their dependence on various PNC properties.

## ASSOCIATED CONTENT

#### Supporting Information

The Supporting Information is available free of charge at https://pubs.acs.org/doi/10.1021/acs.macromol.9b02205.

TEM images showing SiO<sub>2</sub> dispersion in P2VP, ERD/RBS measurements of unannealed PNC films, bound polymer profiles extracted at short times, ERD measurements of bulk P2VP diffusion, and demonstration of restricting NP diffusion (PDF)

## AUTHOR INFORMATION

### **Corresponding Author**

Karen I. Winey — Department of Materials Science and Engineering, University of Pennsylvania, Philadelphia, Pennsylvania 19104, United States; ⊚ orcid.org/0000-0001-5856-3410; Email: winey@seas.upenn.edu

## **Authors**

Eric J. Bailey — Department of Materials Science and Engineering, University of Pennsylvania, Philadelphia, Pennsylvania 19104, United States; orcid.org/0000-0001-7194-9035

Philip J. Griffin – Department of Materials Science and Engineering, University of Pennsylvania, Philadelphia, Pennsylvania 19104, United States

Russell J. Composto — Department of Materials Science and Engineering, University of Pennsylvania, Philadelphia, Pennsylvania 19104, United States; orcid.org/0000-0002-5906-2594

Complete contact information is available at: https://pubs.acs.org/10.1021/acs.macromol.9b02205

#### Notes

The authors declare no competing financial interest.

#### ACKNOWLEDGMENTS

E.J.B., R.J.C., and K.I.W. acknowledge primary support from NSF-CBET #1706014. E.J.B. acknowledges support from the National Science Foundation Graduate Research Fellowship Program under grant no. DGE-1321851. Any opinions, findings, and conclusions or recommendations expressed in this material are those of the authors and do not necessarily reflect the views of the National Science Foundation, R.I.C. acknowledges partial support from ACS/PRF 54028-ND7 and NSF/DMR 1905912. K.I.W. also acknowledges support from the ACS Petroleum Research Fund, 57405-ND7. ERD and RBS measurements were performed at the University of Pennsylvania's Nanoscale Characterization Facility, an NNCI member supported by NSF grant ECCS-1542153, and we thank Doug Yates for assistance with these measurements. The authors also acknowledge facilities support from University of Pennsylvania's MRSEC, NSF grant DMR-1720530. Parts of this work were performed at the Soft Matter Characterization Facility of the University of Chicago. Synthesis of 130 kg/mol dP2VP was conducted at the Center for Nanophase Materials Sciences, which is a DOE Office of Science User Facility. The authors thank Vera Bocharova for NP synthesis and graciously providing NP solutions and Francisco Buitrago for assistance with TEM.

#### REFERENCES

- (1) Kumar, S. K.; Benicewicz, B. C.; Vaia, R. A.; Winey, K. I. 50th Anniversary Perspective: Are Polymer Nanocomposites Practical for Applications? *Macromolecules* **2017**, *50*, 714–731.
- (2) Kumar, S. K.; Ganesan, V.; Riggleman, R. A. Perspective: Outstanding Theoretical Questions in Polymer-Nanoparticle Hybrids. *J. Chem. Phys.* **2017**, *147*, No. 020901.
- (3) Cheng, S.; Carroll, B.; Bocharova, V.; Carrillo, J.-M.; Sumpter, B. G.; Sokolov, A. P. Focus: Structure and Dynamics of the Interfacial Layer in Polymer Nanocomposites with Attractive Interactions. *J. Chem. Phys.* **2017**, *146*, 203201.
- (4) Lin, C.-C.; Parrish, E.; Composto, R. J. Macromolecule and Particle Dynamics in Confined Media. *Macromolecules* **2016**, 49, 5755–5772.
- (5) Holt, A. P.; Bocharova, V.; Cheng, S.; Kisliuk, A. M.; Ehlers, G.; Mamontov, E.; Novikov, V. N.; Sokolov, A. P. Interplay between Local Dynamics and Mechanical Reinforcement in Glassy Polymer Nanocomposites. *Phys. Rev. Mater.* **2017**, *1*, No. 062601.
- (6) Genix, A.-C.; Bocharova, V.; Kisliuk, A.; Carroll, B.; Zhao, S.; Oberdisse, J.; Sokolov, A. P. Enhancing the Mechanical Properties of Glassy Nanocomposites by Tuning Polymer Molecular Weight. ACS Appl. Mater. Interfaces 2018, 10, 33601–33610.
- (7) Merkel, T. C.; Freeman, B. D.; Spontak, R. J.; He, Z.; Pinnau, I.; Meakin, P.; Hill, A. J. Ultrapermeable, Reverse-Selective Nanocomposite Membranes. *Science* **2002**, *296*, 519–522.
- (8) Mogurampelly, S.; Ganesan, V. Influence of Nanoparticle Surface Chemistry on Ion Transport in Polymer Nanocomposite Electrolytes. *Solid State Ionics* **2016**, 286, 57–65.
- (9) Jouault, N.; Zhao, D.; Kumar, S. K. Role of Casting Solvent on Nanoparticle Dispersion in Polymer Nanocomposites. *Macromolecules* **2014**, *47*, 5246–5255.
- (10) Lepcio, P.; Ondreas, F.; Zarybnicka, K.; Zboncak, M.; Caha, O.; Jancar, J. Bulk Polymer Nanocomposites with Preparation Protocol Governed Nanostructure: The Origin and Properties of Aggregates and Polymer Bound Clusters. *Soft Matter* **2018**, *14*, 2094–2103.
- (11) Jouault, N.; Moll, J. F.; Meng, D.; Windsor, K.; Ramcharan, S.; Kearney, C.; Kumar, S. K. Bound Polymer Layer in Nanocomposites. *ACS Macro Lett.* **2013**, *2*, 371–374.

- (12) Jouault, N.; Lee, D.; Zhao, D.; Kumar, S. K. Block-Copolymer-Mediated Nanoparticle Dispersion and Assembly in Polymer Nanocomposites. *Adv. Mater.* **2014**, *26*, 4031–4036.
- (13) Fleer, G. J.; Cohen Stuart, M. A.; Scheutjens, J. M. H.; Cosgrove, T.; Vincent, B. *Polymers at the Interface*; 1st ed.; Chapman and Hall: London, 1993.
- (14) Karatrantos, A.; Clarke, N.; Kröger, M. Modeling of Polymer Structure and Conformations in Polymer Nanocomposites from Atomistic to Mesoscale: A Review. *Polym. Rev.* **2016**, 385–428.
- (15) Jimenez, A. M.; Zhao, D.; Misquitta, K.; Jestin, J.; Kumar, S. K. Exchange Lifetimes of the Bound Polymer Layer on Silica Nanoparticles. ACS Macro Lett. 2019, 8, 166–171.
- (16) Senses, E.; Akcora, P. Tuning Mechanical Properties of Nanocomposites with Bimodal Polymer Bound Layers. *RSC Adv.* **2014**, *4*, 49628–49634.
- (17) Cheng, S.; Holt, A. P.; Wang, H.; Fan, F.; Bocharova, V.; Martin, H.; Etampawala, T.; White, B. T.; Saito, T.; Kang, N.-G.; et al. Unexpected Molecular Weight Effect in Polymer Nanocomposites. *Phys. Rev. Lett.* **2016**, *116*, No. 038302.
- (18) Bailey, E. J.; Griffin, P. J.; Tyagi, M.; Winey, K. I. Segmental Diffusion in Attractive Polymer Nanocomposites: A Quasi-Elastic Neutron Scattering Study. *Macromolecules* **2019**, *52*, 669–678.
- (19) Jouault, N.; Crawford, M. K.; Chi, C.; Smalley, R. J.; Wood, B.; Jestin, J.; Melnichenko, Y. B.; He, L.; Guise, W. E.; Kumar, S. K. Polymer Chain Behavior in Polymer Nanocomposites with Attractive Interactions. *ACS Macro Lett.* **2016**, *5*, 523–527.
- (20) Starr, F. W.; Schrøder, T. B.; Glotzer, S. C. Molecular Dynamics Simulation of a Polymer Melt with a Nanoscopic Particle. *Macromolecules* **2002**, *35*, 4481–4492.
- (21) Robertson, C. G.; Roland, C. M. Glass Transition and Interfacial Segmental Dynamics in Polymer-Particle Composites. *Rubber Chem. Technol.* **2008**, *81*, 506–522.
- (22) Starr, F. W.; Douglas, J. F.; Meng, D.; Kumar, S. K. Bound Layers "Cloak" Nanoparticles in Strongly Interacting Polymer Nanocomposites. *ACS Nano* **2016**, *10*, 10960–10965.
- (23) Gong, S.; Chen, Q.; Moll, J. F.; Kumar, S. K.; Colby, R. H. Segmental Dynamics of Polymer Melts with Spherical Nanoparticles. *ACS Macro Lett.* **2014**, *3*, 773–777.
- (24) Holt, A. P.; Griffin, P. J.; Bocharova, V.; Agapov, A. L.; Imel, A. E.; Dadmun, M. D.; Sangoro, J. R.; Sokolov, A. P. Dynamics at the Polymer/Nanoparticle Interface in Poly(2-Vinylpyridine)/Silica Nanocomposites. *Macromolecules* **2014**, *47*, 1837–1843.
- (25) Holt, A. P.; Bocharova, V.; Cheng, S.; Kisliuk, A. M.; White, B. T.; Saito, T.; Uhrig, D.; Mahalik, J. P.; Kumar, R.; Imel, A. E.; et al. Controlling Interfacial Dynamics: Covalent Bonding versus Physical Adsorption in Polymer Nanocomposites. *ACS Nano* **2016**, *10*, 6843–6852
- (26) Choi, J.; Clarke, N.; Winey, K. I.; Composto, R. J. Polymer Diffusion from Attractive and Athermal Substrates. *Macromolecules* **2017**, *50*, 3038–3042.
- (27) Zheng, X.; Sauer, B. B.; Van Alsten, J. G.; Schwarz, S. A.; Rafailovich, M. H.; Sokolov, J.; Rubinstein, M. Reptation Dynamics of a Polymer Melt near an Attractive Solid Interface. *Phys. Rev. Lett.* **1995**, *74*, 407–410.
- (28) Gin, P.; Jiang, N.; Liang, C.; Taniguchi, T.; Akgun, B.; Satija, S. K.; Endoh, M. K.; Koga, T. Revealed Architectures of Adsorbed Polymer Chains at Solid-Polymer Melt Interfaces. *Phys. Rev. Lett.* **2012**, *109*, 265501.
- (29) Jiang, N.; Cheung, J. M.; Guo, Y.; Endoh, M. K.; Koga, T.; Yuan, G.; Satija, S. K. Stability of Adsorbed Polystyrene Nanolayers on Silicon Substrates. *Macromol. Chem. Phys.* **2018**, *219*, 1700326.
- (30) Senses, E.; Faraone, A.; Akcora, P. Microscopic Chain Motion in Polymer Nanocomposites with Dynamically Asymmetric Interphases. *Sci. Rep.* **2016**, *6*, 29326.
- (31) Jiang, N.; Endoh, M. K.; Koga, T.; Masui, T.; Kishimoto, H.; Nagao, M.; Satija, S. K.; Taniguchi, T. Nanostructures and Dynamics of Macromolecules Bound to Attractive Filler Surfaces. *ACS Macro Lett.* **2015**, *4*, 838–842.

- (32) Voylov, D. N.; Holt, A. P.; Doughty, B.; Bocharova, V.; Meyer, H. M., III; Cheng, S.; Martin, H.; Dadmun, M.; Kisliuk, A.; Sokolov, A. P. Unraveling the Molecular Weight Dependence of Interfacial Interactions in Poly(2-Vinylpyridine)/Silica Nanocomposites. *ACS Macro Lett.* **2017**, *6*, 68–72.
- (33) Papon, A.; Montes, H.; Lequeux, F.; Oberdisse, J.; Saalwächter, K.; Guy, L. Solid Particles in an Elastomer Matrix: Impact of Colloid Dispersion and Polymer Mobility Modification on the Mechanical Properties. *Soft Matter* **2012**, *8*, 4090–4096.
- (34) Napolitano, S.; Wübbenhorst, M. The Lifetime of the Deviations from Bulk Behaviour in Polymers Confined at the Nanoscale. *Nat. Commun.* **2011**, *2*, 260.
- (35) Kamiya, H.; Suzuki, H.; Kato, D.; Jimbo, G. Densification of Alkoxide-Derived Fine Silica Powder Compact by Ultra-High-Pressure Cold Isostatic Pressing. *J. Am. Ceram. Soc.* **1993**, *76*, 54–64.
- (36) Iijima, M.; Kamiya, H. Layer-by-Layer Surface Modification of Functional Nanoparticles for Dispersion in Organic Solvents. *Langmuir* **2010**, *26*, 17943–17948.
- (37) Griffin, P. J.; Bocharova, V.; Middleton, L. R.; Composto, R. J.; Clarke, N.; Schweizer, K. S.; Winey, K. I. Influence of the Bound Polymer Layer on Nanoparticle Diffusion in Polymer Melts. *ACS Macro Lett.* **2016**, *5*, 1141–1145.
- (38) Composto, R. J.; Walters, R. M.; Genzer, J. Application of Ion Scattering Techniques to Characterize Polymer Surfaces and Interfaces. *Mater. Sci. Eng., R* **2002**, *38*, 107–180.
- (39) Gam, S.; Meth, J. S.; Zane, S. G.; Chi, C.; Wood, B. A.; Seitz, M. E.; Winey, K. I.; Clarke, N.; Composto, R. J. Macromolecular Diffusion in a Crowded Polymer Nanocomposite. *Macromolecules* **2011**, *44*, 3494–3501.
- (40) Bailey, E. J.; Griffin, P. J.; Composto, R. J.; Winey, K. I. Multiscale Dynamics of Small, Attractive Nanoparticles and Entangled Polymers in Polymer Nanocomposites. *Macromolecules* **2019**, *52*, 2181–2188.
- (41) Tung, W.-S.; Griffin, P. J.; Meth, J. S.; Clarke, N.; Composto, R. J.; Winey, K. I. Temperature-Dependent Suppression of Polymer Diffusion in Polymer Nanocomposites. *ACS Macro Lett.* **2016**, 735–739
- (42) Lin, C.-C.; Gam, S.; Meth, J. S.; Clarke, N.; Winey, K. I.; Composto, R. J. Do Attractive Polymer—Nanoparticle Interactions Retard Polymer Diffusion in Nanocomposites? *Macromolecules* **2013**, 46, 4502–4509.
- (43) Kramer, E. J.; Green, P.; Palmstrøm, C. J. Interdiffusion and Marker Movements in Concentrated Polymer-Polymer Diffusion Couples. *Polymer* **1984**, *25*, 473–480.
- (44) Gam, S.; Meth, J. S.; Zane, S. G.; Chi, C.; Wood, B. A.; Winey, K. I.; Clarke, N.; Composto, R. J. Polymer Diffusion in a Polymer Nanocomposite: Effect of Nanoparticle Size and Polydispersity. *Soft Matter* **2012**, *8*, 6512–6520.
- (45) Chen, Q.; Gong, S.; Moll, J.; Zhao, D.; Kumar, S. K.; Colby, R. H. Mechanical Reinforcement of Polymer Nanocomposites from Percolation of a Nanoparticle Network. *ACS Macro Lett.* **2015**, 398–402
- (46) Green, P. F.; Kramer, E. J. Matrix Effects on the Diffusion of Long Polymer Chains. *Macromolecules* **1986**, *19*, 1108–1114.
- (47) Yamamoto, U.; Schweizer, K. S. Microscopic Theory of the Long-Time Diffusivity and Intermediate-Time Anomalous Transport of a Nanoparticle in Polymer Melts. *Macromolecules* **2015**, *48*, 152–163.
- (48) Yamamoto, U.; Carrillo, J.-M. Y.; Bocharova, V.; Sokolov, A. P.; Sumpter, B. G.; Schweizer, K. S. Theory and Simulation of Attractive Nanoparticle Transport in Polymer Melts. *Macromolecules* **2018**, *51*, 2258–2267.
- (49) Agapov, A. L.; Novikov, V. N.; Hong, T.; Fan, F.; Sokolov, A. P. Surprising Temperature Scaling of Viscoelastic Properties in Polymers. *Macromolecules* **2018**, *51*, 4874–4881.
- (50) Li, Y.; Kröger, M.; Liu, W. K. Nanoparticle Effect on the Dynamics of Polymer Chains and Their Entanglement Network. *Phys. Rev. Lett.* **2012**, *109*, 118001.